AECL EACL

Conference Paper

PREDICTION OF METAL OXIDE STABILITY IN SUPERCRITICAL WATER REACTORS-POURBAIX VERSUS ELLINGHAM

COMPANY WIDE

CW-127120-CONF-006

Revision 0

Prepared by
Rédigé par

Reviewed by
Vérifié par

Approved by
Approuvé par

2013/09/25

UNRESTRICTED

2013/09/25

ILLIMITÉ

Chalk River, Ontario
Canada K0J 1J0

Chalk River (Ontario)
Canada K0J 1J0

PREDICTION OF METAL OXIDE STABILITY IN SUPERCRITICAL WATER REACTORS-POURBAIX VERSUS ELLINGHAAM

L. Qiu and D.A. Guzonas

Atomic Energy of Canada Limited, Chalk River, Ontario, Canada

Abstract

Knowledge of the thermodynamic stabilities of metals and their oxides is important for understanding material degradation and corrosion product transport in a supercritical water-cooled reactor (SCWR). The thermodynamic stability under various conditions can be illustrated using graphical representations such as Pourbaix and Ellingham diagrams. This paper will show how a combination of Pourbaix and Ellingham diagrams is necessary to characterize the thermodynamic stability of alloys and oxide films under proposed SCWR coolant conditions. Results predicted using both Pourbaix and Ellingham diagrams will be compared with literature data. The advantages and disadvantages of these methods under SCWR conditions will also be discussed.

1. Introduction

The proposed Canadian-SCWR is designed to operate with core inlet and outlet temperatures of 350 and 625 ^{o}C, respectively. Knowledge of the thermodynamic stability of the materials of construction (mainly Fe-Ni-Cr alloys) and their corrosion products under these conditions is required for the prediction of material degradation and corrosion product transport. Stability can be evaluated by direct thermodynamic calculations or from graphical representations such as Pourbaix or Ellingham diagrams. These diagrams are useful for identifying thermodynamically stable phases and locating immune regions of a metal or alloy under reducing and oxidizing conditions.

Pourbaix (electrical potential versus pH) diagrams are constructed using thermodynamic data by means of the Nernst equation, and are valuable at low temperatures where reliable thermodynamic data for ions and their hydrolysis species are available. As the temperature increases, especially approaching the critical point of water (374 ^{o}C, 22.06 MPa), the identification of hydrolysis species becomes a challenge and the required thermodynamic data for these species are rarely available. Consequently, empirical methods are often used to extrapolate data from lower temperatures (usually below 100 ^{o}C) to high temperatures, including the supercritical region. In many cases, the uncertainties in the values of thermodynamic parameters obtained by extrapolation cannot be reliably estimated because of a lack of experimental data, and the resulting Pourbaix diagrams can be misleading. Most importantly, at temperatures just above the critical point, the physical and chemical properties of water change drastically and water behaves like a non-polar solvent. Above the critical point, the dissociation of supercritical water (SCW) decreases significantly and reliable pH measurements are very difficult, making the significance of pH as a chemistry parameter unclear. Marrone and Hong suggested that at temperatures above about 400 °C, Pourbaix diagrams become unsuitable for depicting the thermodynamic stability of metals and their oxides [1].

At these higher temperatures, Ellingham diagrams, presenting the standard Gibbs energy change of a chemical reaction as a function of temperature, are more suitable thermodynamic constructs. These

diagrams avoid the ambiguities surrounding the definition and measurement of pH in SCW, and are widely used in the metals industry to select reducing agents, purify metals and identify oxide stable regions. Most importantly, the thermodynamic data for many high temperature gas-solid reactions relevant to SCWR materials are available from the literature, which make it much easier to construct reliable Ellingham diagrams.

This paper will show how both Pourbaix and Ellingham diagrams are needed to fully describe the thermodynamic stability of alloys and oxide films under proposed SCWR coolant conditions. Results predicted using both Pourbaix and Ellingham diagrams will be compared with experimental measurements from the literature. The advantages and disadvantages of these methods for the prediction of the thermodynamic stability of alloys and their oxides in SCW will also be discussed.

2. Physical and chemical properties of subcritical and supercritical water

The core inlet temperature of the Canadian SCWR concept is 350 ^{o}C; at this temperature, pK_w is near a minimum and water is much more dissociable than at room temperature (Figure 1) [2]. Hence, ions (and their reactions including hydrolysis) are important solution species at the core inlet, and the stability of metals and metal oxides in this region can be well described using Pourbaix diagrams.

The coolant passes from the subcritical to the supercritical state in the core (T_c = 374 ^{o}C, P_c = 22.01 MPa, Figure 2); while there is no phase change, the transition is similar in some respects to the liquid-vapour transition below the critical point, with a sharp heat capacity change around the transition temperature [3]. Just above the critical point, water is still quite dissociable. The pH (i.e., 1/2 pK_w; K_w is the self-dissociation constant of water) of pure water at 380 ^{o}C and 25 MPa is 6.8, similar to that of water at room temperature, and ionic species are still important. However, the dielectric constant of water (ε = 6.18) at 400 ^{o}C is much lower than that of room temperature water, being similar to that of liquid H_2S (ε = 5.93 at 10 ^{o}C) and acetic acid (ε = 6.2 at 20 ^{o}C) but still much greater than the value for gases and low pressure, high temperature steam (e.g. about 1 at 1 MPa, 500 ^{o}C) [4]. In this region the density of SCW (Figure 3) [3] is between that of high temperature liquid water (ρ=0.63 at 350 ^{o}C, 10 MPa) and low pressure steam (ρ = 0.045 at 350 ^{o}C, 10 MPa).

As the temperature increases above 400 ^{o}C, K_w decreases rapidly and water dissociation becomes negligible. The value of pK_w at 410 ^{o}C is a factor of 6 lower than the value at 380 ^{o}C and four times lower than that of room temperature ethanol (pK_a =16 at 25^{o}C) [4]. The SCWR coolant above 400 ^{o}C is therefore virtually un-dissociable and the utility of pH as a chemistry parameter is limited. It should be noted that the pK_w and other SCW properties are also a function of pressure, and SCW becomes more dissociable as the pressure increases at constant temperature.

The density of SCW above 400 ^{o}C decreases almost linearly with increasing temperature at constant pressure. The density at which the physical properties of SCW change from liquid-like to gas-like can be estimated from the crossover point of the dashed lines of the density curves (Figure 3); a value of about 100 kg/m^3 is obtained. This corresponds to a transition temperature of about 460 °C. The transition temperature is dependent on pressure, i.e., as the pressure of the system increases, the transition temperature also increases. The gas-like nature of low density SCW is reflected by many other physical properties; e.g., the entropy shows almost no difference between SCW and high temperature steam above 400 ^{o}C.

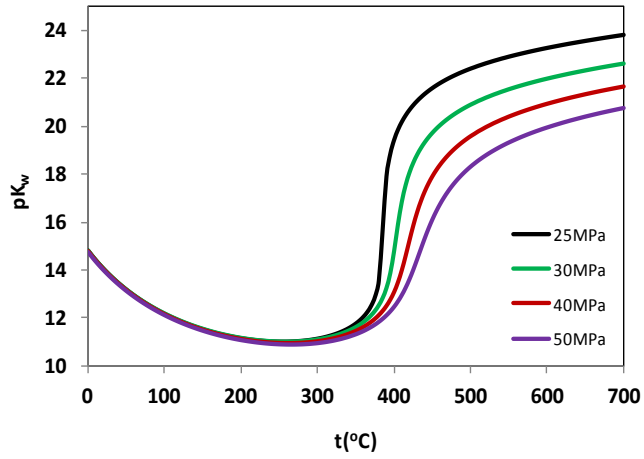

Figure 1: Ion Product of pure water as a function of temperature.

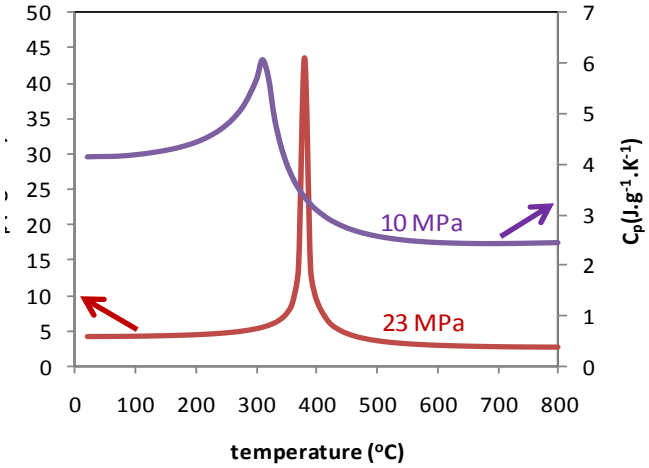

Figure 2: Heat capacity of pure water as a function of temperature.

The gas-like nature of low-density SCW can be assessed by fitting SCW properties by an equation of state for gases. Figure 4 shows the SCW pressure calculated using the van der Waals equation ($P = \frac{RT}{(V_m - b)} - \frac{a}{V_m^2}$,) and literature values for the density [3] at 25 MPa. The constants $a = \frac{27R^2T_c^2}{64P_c}$ and $b = \frac{RT_c}{8P_c}$ are 5.406 and 0.03016, respectively, as calculated from T_c and P_c of water. The calculated pressure agrees with literature data within an uncertainty of 4.1% as shown in Figure 4. Below 500 °C, the predicted and measured pressures begin to converge and below 400 °C the van der Waals equation is no longer reliable. The results calculated using the ideal gas equation are also shown in Figure 4 for comparison. Above 700 °C, SCW has a compressibility $Z = \frac{PV_m}{RT}$ close to 1, as expected for an ideal gas.

The distinction between liquid-like (high density) and gas-like (low density) SCW is important because the thermodynamic stability of oxides, corrosion mechanisms, and corrosion product and activity transport behavior depend on the physical and chemical properties of water, which in turn depend on density. For example, the corrosion of stainless steel in high density SCW is similar to that in subcritical high temperature water while corrosion in low density SCW is similar to wet air oxidation [5, 6]. Corrosion products (including radionuclides) in liquid-like SCW are transported by oxide dissolution to give ionic species in solution, while in low-density SCW these species are transported by formation of neutral hydrated species at the metal or metal oxide surface followed by evaporation. In the latter case mass transport depends on the volatility or distribution coefficient of species between the gas and solid phases as well as their thermodynamic stability in the gas phase. In SCW the terms dissolution and evaporation are largely interchangeable.

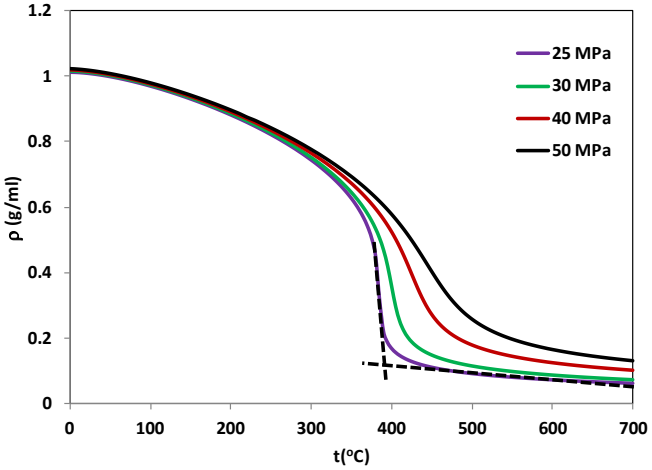

Figure 3: Density of water as a function of temperature.

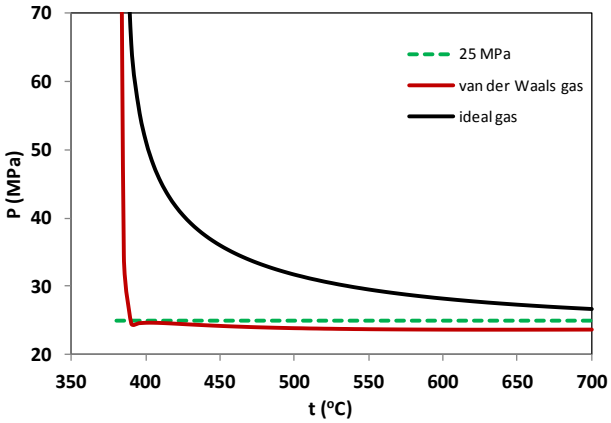

Figure 4: Calculated SCW pressure using van der Waals and ideal gas equations.

3. Prediction of oxide stability in SCWR from Pourbaix diagrams

Poubaix diagrams for subcritical water have been extensively studied. These diagrams are constructed using the Nernst equation, $\Delta G = -nFE$, combined with empirical techniques such as the Criss and Cobble method [7] to estimate the heat capacities of redox species in the electrode reactions. Examples for Fe-H_2O and Ni-H_2O [8] at 300 ^oC are shown in Figures 5 and 6. Ionic and hydrolysis species are predicted to be stable under these conditions and the Pourbaix diagram for iron corresponds well with solubility measurements of iron oxides [9-11].

A few Pourbaix diagrams in the near critical or supercritical region have been constructed using the Helgeson-Kirkham-Flowers (HKF) model [12, 13]. Figure 7 shows the Pourbaix diagram for the Fe-H_2O system at 400 ^oC and 30 MPa and an iron activity of 10^{-6} M [12]. Under strongly reducing conditions, metallic iron is stable, while at a pH greater than 6 and relatively weak reducing conditions, Fe_3O_4 is stable, in agreement with data on oxide films formed in SCW. Under oxidizing conditions, Fe_2O_3 is the stable phase. FeO was not included in the diagram because the authors believed this phase to be unstable with respect to Fe and Fe_3O_4 below 560 ^oC. Compared with the Pourbaix diagrams for the Fe-H_2O system under subcritical conditions (Figure 5), the regions of stability of ionic species are much smaller and exist only at acidic pH values.

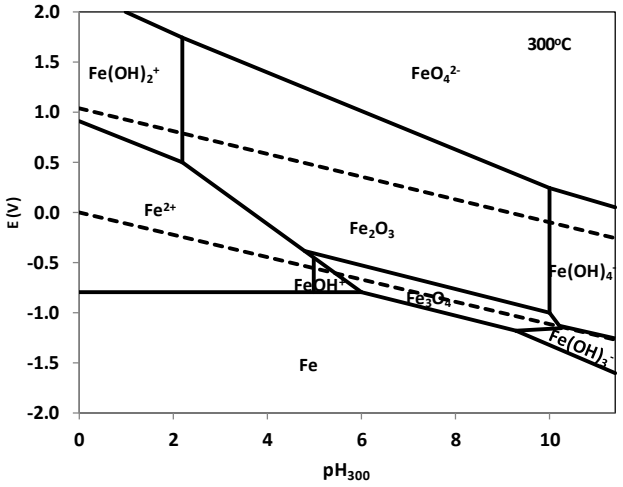

Figure 5: Pourbaix diagram for Fe at 300 °C [8].

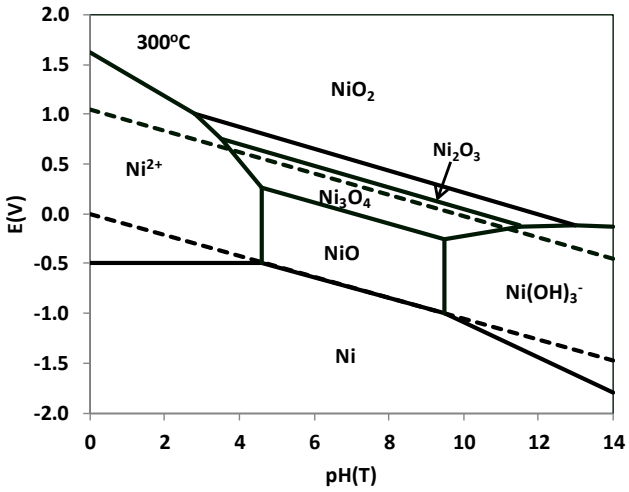

Figure 6: Pourbaix diagram for Ni at 300 °C [8].

Pourbaix diagrams for nickel in SCW have been calculated by several groups [14, 15] and the results are very similar. Figure 8 shows the Pourbaix diagram for the Ni-H_2O system near the critical point; dissolved nickel ion is predicted to be the dominant species below pH(T) 4.5. NiO is predicted to be the stable phase under reducing conditions at pH(T) greater than 4.5. Other nickel oxides (Ni_3O_4, Ni_2O_3 and NiO_2) are possible under oxidizing conditions.

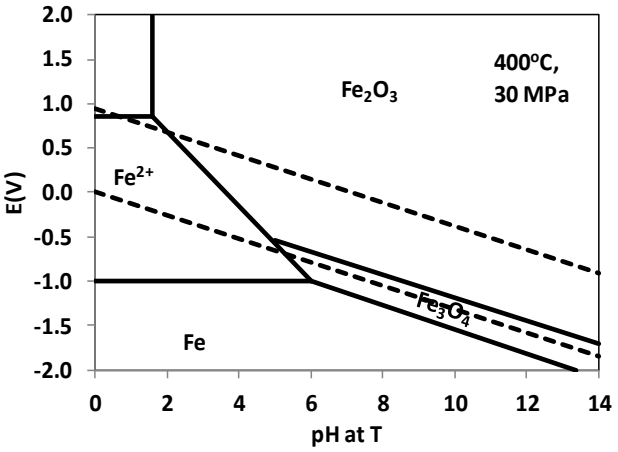

Figure 7: Pourbaix diagrams for Fe in SCW.

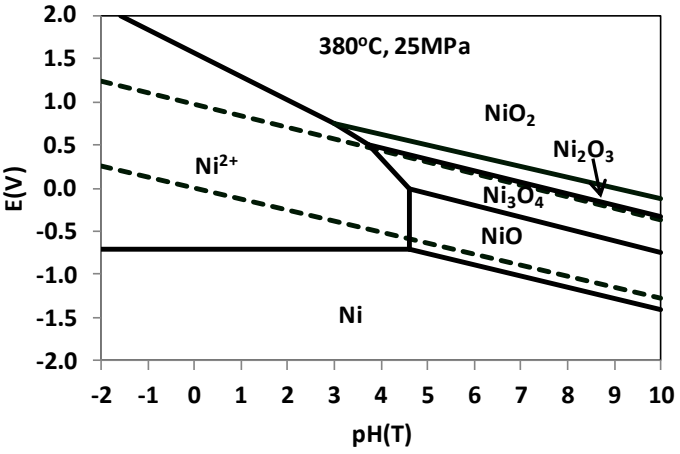

Figure 8: Pourbaix diagram for Ni in SCW.

A common characteristic of the Pourbaix diagrams in SCW is that the phases do not generally change at pH values greater than 6, indicating that the pH of SCW does not affect the stability of oxides in weak acidic and alkaline SCW due to the low dissociation of water. It should be noted that the pressure of Pourbaix diagrams constructed for SCW is often greater than 25 MPa so that a liquid-like density of SCW can be retained (e.g., Figure 7). At the proposed SCWR operating pressure of 25 MPa, the dissociation of water is lower and small changes in pH will have less effect on corrosion products

as only metals and oxides are stable. Consequently, at the higher temperatures Pourbaix and Ellingham diagrams predict essentially the same phase diagrams for metal and oxides.

4. Application of Ellingham diagrams to corrosion in an SCWR

At temperatures well above T_c, the concentrations of ionic and hydration species are very low and Ellingham diagrams can be used to predict the thermodynamic stability of metal and oxides. For a gas-phase metal oxidation reaction,

$$\frac{2n}{m} M + O_2 = \frac{2}{m} M_n O_m \quad (1)$$

the Gibbs energy change is:

$$\Delta G^0 = -RTlnK \quad (2)$$

where ΔG^0 is the standard Gibbs energy change at the reaction temperature T. The equilibrium constant K of the chemical reaction can be expressed as

$$K = p(O_2), \quad (3)$$

and

$$\Delta G^o = RTln(p(O_2)) \quad (4)$$

where $p(O_2)$ is the partial pressure of O_2 at reaction equilibrium. An example of an Ellingham diagram for metal oxidation is shown in Figure 9. It should be noted that the y-axis in an Ellingham diagram is the Gibbs energy change of oxidation reaction (1) per mole of O_2 consumed so that a comparison of the thermodynamic stability of different phases can be carried out under same conditions.

Ellingham diagrams are particularly useful for comparison of the relative thermodynamic stability of the multiple elements (and their oxides) in the alloys under various redox conditions. In Ellingham diagrams, the Gibbs energy changes increase from bottom to top. This corresponds to the electrode potential increase in a Pourbaix diagram, since electrode potential is directly linked to the negative of the Gibbs energy changes by the Nernst equation. Figure 9 shows that at the same temperature, zirconium, titanium and chromium are easily oxidized due to their lower Gibbs energy changes while nickel appears to be the most stable metal. Experiments confirm that nickel and nickel alloys have low corrosion rates under SCWR conditions [16] compared to those of zirconium [17] and titanium [18]. Unlike Pourbaix diagrams, ionic species are not shown because they are not stable in low density SCW.

The thermodynamic stability of iron and its oxides is a key parameter in determining the stability of alloys to be used in the SCWR core and is shown in Figure 10. Elemental Fe, magnetite (Fe_3O_4) and hematite (Fe_2O_3) are three possible phases below 600 ^oC and the stability of each phase depends on the oxidizing condition. Under strong reducing conditions or low O_2 concentrations, Fe is stable. As the oxygen partial pressure increases, Fe can be oxidized to magnetite. Under strongly oxidizing conditions (high $p(O_2)$), the stable phase of iron is hematite. The same results are obtained from the

Pourbaix diagram for Fe in SCW (Figure 7). As the temperature increases above 600 °C, FeO is also predicted to be stable.

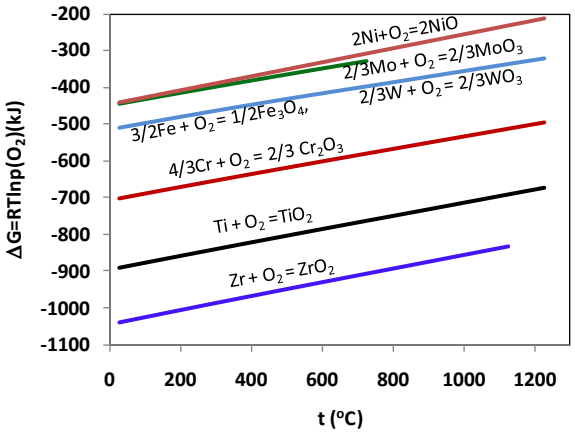

Figure 9: Ellingham diagram for metal oxidation.

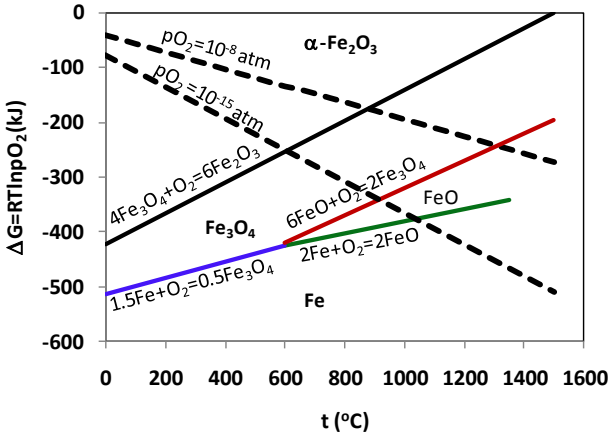

Figure 10: Ellingham diagram for the Fe system.

Figure 11 shows the Ellingham diagram of the nickel system using literature values for $\Delta_f G_m^o(298K)$ and $S_m^o(298K)$ [15, 19, 20]. Comparing the stability of nickel oxide phases in the Ellingham diagram with those in the Pourbaix diagram at the same temperature and pressure (400 °C, 25 MPa, Figure 11) [21] shows that the predicted phases and order of stability are the same. As pH is not an important parameter in the low-density region of the SCWR core, the stability of oxides in this region can be completely represented by Ellingham diagrams.

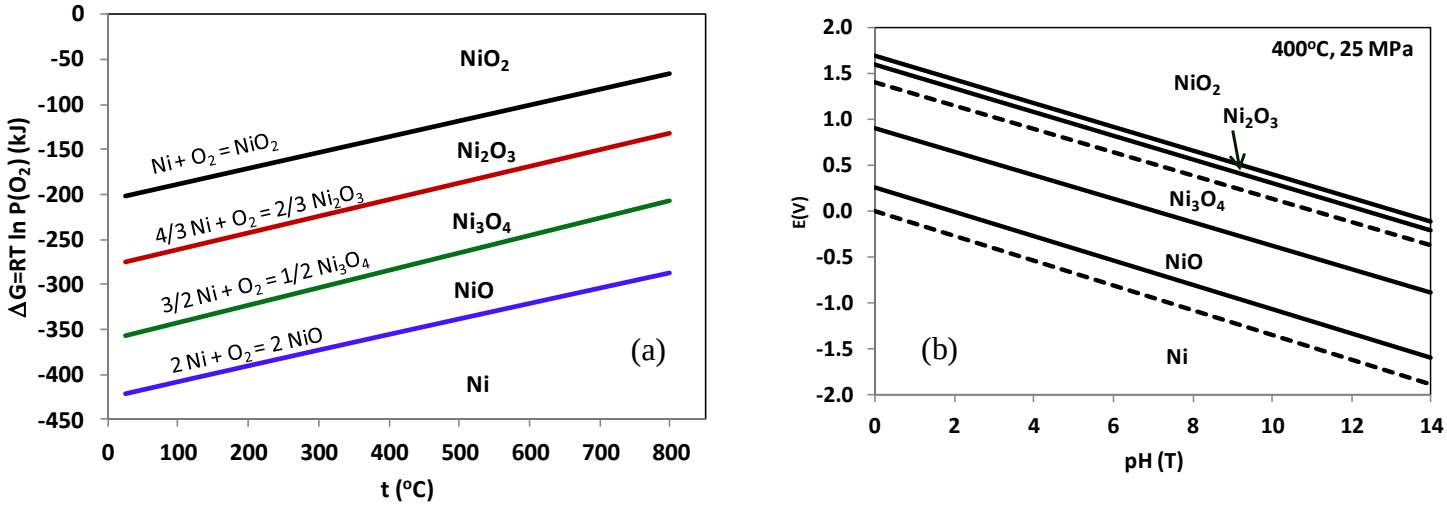

Figure 11: Comparison of Ellingham (a) and Pourbaix (b) diagrams for the Ni system. Pourbaix diagram based on [19].

Ellingham diagrams show some flexibility over Pourbaix diagrams in choice of variables on the *x*- and *y*-axis. Figure 12 shows the Ni-H_2-H_2O phase diagram in supercritical water system with log p(H_2O)

as the x-axis and log $p(H_2)$ as the y-axis. The phase diagram was constructed based on the three reaction equilibria:

$$NiO + H_2O\ (g) = Ni(OH)_2, \qquad K_1 = \frac{1}{p(H_2O)} \tag{5}$$

$$NiO + H_2 = Ni + H_2O\ (g), \qquad K_2 = \frac{p(H_2O)}{p(H_2)} \tag{6}$$

$$Ni(OH)_2 + H_2 = Ni + 2H_2O\ (g), \qquad K_3 = \frac{(p(H_2O))^2}{p(H_2)} \tag{7}$$

The values of *K* can be calculated from the Gibbs energy changes of each reaction [1]. At 650 ^oC and 25 MPa, $Ni(OH)_2$ is predicted to be the stable solid phase, consistent with corrosion tests [22]. However, Marrone and Hong [1] thought that both NiO and $Ni(OH)_2$ are possible considering the non-idealities in SCW systems.

Ellingham diagrams are especially useful in low density SCW (high temperature superheated steam) as the concentration effects of H_2, O_2 on the stability of metal and corrosion product can be identified directly (Figures 10 and 13). In multi-component steam, the equilibrium constant and Gibbs energy change of H_2 oxidation can be expressed as

$$2H_2\ (g) + O_2\ (g) = 2H_2O\ (g) \tag{8}$$

$$K_p = \frac{[p(H_2O)]^2}{[p(H_2)]^2 \cdot p(O_2)} \tag{9}$$

and

$$\Delta G^o = -RTlnK_p \tag{10}$$

or

$$RTlnp(O_2) = \Delta G^o + 2RTln\left[\frac{p(H_2O)}{p(H_2)}\right] \tag{11}$$

Equation (11) is shown in Figure 13 (dashed lines). The thermodynamic stability of the Cr oxidation reaction

$$\frac{4}{3}Cr + O_2 = \frac{2}{3}Cr_2O_3 \tag{12}$$

is also shown in the figure (solid line). The overall Gibbs energy change between reactions (8) and (12) is determined using equations (13) and (14)

$$\frac{4}{3}Cr + 2\,H_2O = \frac{2}{3}Cr_2O_3 + 2H_2 \quad (13)$$

and

$$\Delta G = \Delta G_f^o\left(\frac{2}{3}Cr_2O_3\right) - \Delta G_f^o(2H_2O) + 2RTln\left[\frac{p(H_2O)}{p(H_2)}\right] \quad (14)$$

When the (dashed) line representing hydrogen oxidation crosses the (solid) line representing chromium oxidation, the chromium and hydrogen oxidation reactions are in equilibrium and their Gibbs energies are the same. When the solid line at a particular temperature is above the dashed line, chromium oxide will be reduced spontaneously by hydrogen to chromium metal, i.e., under such conditions, chromium metal is stable than chromium oxide. For example, if $p(H_2O)/p(H_2) = 10^{-10}$, chromium metal is stable above 400 ^oC. In the Canadian SCWR, the partial pressure of hydrogen is expected to be much smaller than the water pressure and chromium will be present as Cr_2O_3.

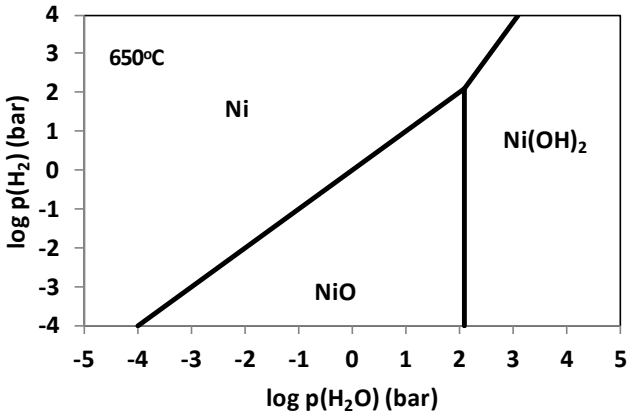

Figure 12: Ellingham diagram for the Ni-H_2-H_2O system at 650 ^oC.

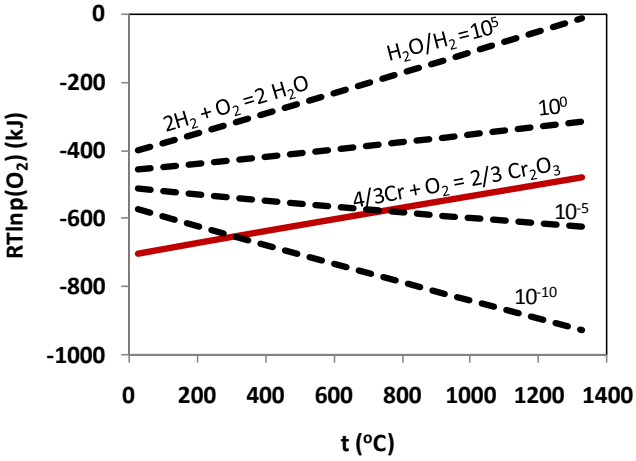

Figure 13: Ellingham diagram for the Cr-O_2-H_2-H_2O system

5. Summary

Pourbaix and Ellingham diagrams are both thermodynamic constructs derived from the Gibbs energy change and used to predict the stability of metals and metal oxides. As the temperature of the SCW coolant changes from subcritical to supercritical and the physical properties of the coolant changes from liquid-like to gas-like, water dissociation decreases dramatically and pH is no longer a useful variable. A complete description of the thermodynamic stability of metals and metal oxides and the associated solution species in an SCWR therefore requires both Pourbaix and Ellingham diagrams. Consideration of the physical properties of SCW suggests that the transition occurs at an SCW density of about 100 kg/m^3, which corresponds to about 460 ^oC at the proposed SWCR operating pressure of 25 MPa. Under conditions where ionic species and water dissociation are not important, the results predicted by Pourbaix and Ellingham diagrams are the same.

It is important to note that, as thermodynamic methods, neither diagram provides information about the kinetics; for example, the dissolution rate of an oxide film on a metal surface cannot be inferred from these diagrams. Therefore these diagrams should be used only as a guide to understanding experimental data when assessing corrosion susceptibility in an SCWR.

6. References

[1] P.A. Marrone and G.T. Hong, "Corrosion Control Methods in Supercritical Water Oxidation and Gasification Process", Journal of Supercritical Fluids, Vol. 51, 2009, pp. 83-103.

[2] W.L. Marshall and E.U. Franck, "Ion Product of Water Substance, 0-1000^{o}C, 1-10,000 Bars, New International Formulation and its Background", Journal of Physical and Chemical Reference Data, Vol. 10, 1981, Iss. 2, pp. 295-304.

[3] L. Harr, J.S. Gallagher and G.S. Kell, "NBS/NRC Steam Tables-Thermodynamic and Transport Properties and Computer Programs for Vapor and Liquid States of Water in SI Units", Hemisphere Publishing Corporation, Washington, 1984.

[4] D.R. Lide, "CRC Handbook of Chemistry and Physics", 89th Edition, CRC Press, New York, 2008.

[5] I. Betova, M. Bojinov, P. Kinnunen, S. Penttilä, and T. Saario, "Surface Film Electrochemistry of Austenitic Stainless Steel and Its Main Constituents in Supercritical Water", Journal of Supercritical Fluids, Vol. 43, 2007, pp. 333-340.

[6] D.A. Guzonas and W.G. Cook, "Corrosion in a Supercritical Water-cooled Reactor – Developing a Mechanistic Framework", The 3rd China-Canada Joint Workshop on Supercritical-Water-Cooled Reactors, CCSC-2012, Xi'an, China, April 18-20, 2012.

[7] C.M. Criss, and J.W. Cobble, "The Thermodynamic Properties of High Temperature Aqueous Solutions. V. The Calculation of Ionic Capacities up to 200^{o}C. Entropies and Heat Capacities above 200^{o}C", Journal of American Chemical Society, Vol. 86, 1964, pp. 5385-8390.

[8] B. Beverskog and I.Puigdomenech, "Revised Pourbaix Diagrams for Iron at 25-300^{o}C", Corrosion Science, Vol. 38, No. 12, 1996, pp. 2121-2135.

[9] F.H. Sweeton, and C.F. Baes, Jr., "Solubility of Magnetite and Hydrolysis of Ferrous Ion in Aqueous Solutions at Elevated Temperatures", Journal of Chemical Thermodynamics, Vol. 2, 1970, pp. 479-500.

[10] P.R. Tremaine and J.C. LeBlanc, "The Solubility of Magnetite and the Hydrolysis and Oxidation of Fe^{2+} in Water to 300^{o}C", Journal of Solution Chemistry, Vol. 9, No.6, 1980, pp. 415.

[11] S.E. Ziemniak, M.E. Jones, and K.E.S. Combs, "Magnetite Solubility and Phase Stability in Alkaline Media at Elevated Temperatures", Journal of Solution Chemistry, Vol. 24, No. 9, 1995, pp. 837-877.

[12] L.B. Kriksunov and D.D. Macdonald, "Potential-pH Diagrams for Iron in Supercritical Water", Corrosion, Vol. 53, 1997, 605-611.

[13] W.A. Propp, T.E. Carleson, C.M. Wai, P.R. Taylor, K.W. Daehling, S. Huang, M.A. Latif, "Corrosion in Supercritical Fluids", Idaho National Engineering Laboratory, INEL-96/0180, 1996.

[14] D.D. Macdonald and L.B. Kriksunov, "Probing the Chemical and Electrochemical Properties of SCWO Systems", Electrochimica Acta, Vol. 47, 2001, pp. 775-790.

[15] G.S. Was, P. Ampornrat, G. Gupta, S. Teysseyre, E.A. West, T.R. Allen, K. Sridharan, L. Tan, Y. Chen, X. Ren, C. Pister, "Corrosion and Stress Corrosion Cracking in Supercritical Water", J. Nucl. Mater. Vol. 371, 2007, 176-201.

[16] D.A. Guzonas, J. Wills, and L. Qiu, "Chemistry and Materials Issues in a Supercritical Water CANDU® Reactor", Proceedings in China-Canada Joint Workshop of SCWR (CCSC2008), Shanghai, China, 2008 April 25-26.

[17] A.T. Motta, A.Yilmazbayhan, M.J. Gomes da Silva, R.J. Comstock, G.S. Was, J.T. Busby, E.Gartner, Q. Peng, Y.H. Jeong, J.Y. Park, "Zirconium Alloys for Supercritical Water Reactor Applications: Challenges and Possibilities", J. Nucl. Mater. Vol. 371 2007, 61–75.

[18] J. Kaneda, S. Kasahara, J. Kuniya, K. Moriya, F. Kano, N. Saito, A. Shioiri, T. Shibayama, H. Takahashi, "General Corrosion Properties of Titanium Based Alloys for the Fuel Claddings in the Supercritical Water-Cooled Reactor", Proceedings of the 12th International Conference on Environmental Degradation of Materials in Nuclear Power Systems – Water Reactors, 2006; pp 1409–1419.

[19] B.S. Hemingway, "Thermodynamic Properties for Bunsenite, NiO, Magnetite, Fe_3O_4, Hematite, Fe_2O_3 with Comments on Selected Oxygen Buffer Reactions", American Mineralogist, Vol. 75, 1990, pp.781-790.

[20] H. Gamsjager and F.J. Mompean, "Chemical Thermodynamics of Nickel", Elsevier, Amsterdam, 2005.

[21 W.G. Cook and R.P. Olive, "Pourbaix Diagrams for the Nickel-Water System Extended to High-Subcritical and Low Supercritical Conditions", Corrosion Science, to be published, 2012.

[22] M. C. Sun, X. Q. Wu, Z. E. Zhang, E. H. Han, "Analyses of Oxide Films Grown on Alloy 625 in Oxidizing Supercritical Water", Journal of Supercritical Fluids, Vol. 47, 2008, pp. 309-317.